

# JGR Space Physics

## RESEARCH ARTICLE

10.1029/2020JA028860

### Special Section:

Cluster 20th anniversary: re-  
sults from the first 3D mission

### Key Points:

- A thin electron current layer is embedded within a broader ion-scale current layer in the trailing part of magnetosheath magnetic peak
- Direct evidence of magnetic reconnection is found inside the thin electron current layer of magnetic peak
- Electrons are significantly heated in two regions of peaks: reconnecting current layer and trailing edges, in different mechanisms

### Correspondence to:

R. Wang and Q. Lu,  
[rswan@ustc.edu.cn](mailto:rswan@ustc.edu.cn);  
[qmlu@ustc.edu.cn](mailto:qmlu@ustc.edu.cn)

### Citation:

Wang, S., Wang, R., Lu, Q., Burch, J. L., & Wang, S. (2021). Energy dissipation via magnetic reconnection within the coherent structures of the magnetosheath turbulence. *Journal of Geophysical Research: Space Physics*, 126, e2020JA028860. <https://doi.org/10.1029/2020JA028860>

Received 23 OCT 2020

Accepted 15 MAR 2021

© 2021. American Geophysical Union.  
All Rights Reserved.

## Energy Dissipation via Magnetic Reconnection Within the Coherent Structures of the Magnetosheath Turbulence

Shimou Wang<sup>1,2,3</sup> , Rongsheng Wang<sup>1,2,3</sup> , Quanming Lu<sup>1,2,3</sup> , J. L. Burch<sup>4</sup> , and Shui Wang<sup>1,2,3</sup>

<sup>1</sup>CAS Key Laboratory of Geospace Environment, Department of Geophysics and Planetary Science, University of Science and Technology of China, Hefei, China, <sup>2</sup>CAS Center for Excellence in Comparative Planetology, Hefei, China, <sup>3</sup>Anhui Mengcheng Geophysics National Observation and Research Station, University of Science and Technology of China, Mengcheng, China, <sup>4</sup>Southwest Research Institute, San Antonio, TX, USA

**Abstract** A series of intermittent coherent structures was observed in magnetosheath turbulence in the form of magnetic peaks. These magnetic peaks are always accompanied with enhancement of local current density, and three of them are studied in detail because of their intense current density. Based on the magnetic field signals, magnetic curvatures, and the toroidal magnetic field lines, three peaks are identified as magnetic flux ropes. In each trailing part of these three peaks, an extremely thin electron current layer was embedded within a much broader ion-scale current layer. The energy dissipation is evident within the peaks and direct evidence of magnetic reconnection was found within the thinnest electron current layer. The electrons were heated mainly in two regions of magnetic peaks, that is, the reconnecting current layer by parallel electric field and the trailing edges by Fermi and betatron mechanisms. These results suggest that the ion-scale magnetic peaks are coherent structures associated with energy dissipation and electron heating in the magnetosheath. Thin current layers can be formed in magnetic peaks, and magnetic reconnection can play a significant role for the energy dissipation in magnetic peaks.

**Plain Language Summary** Turbulence is important in transferring energy from large scales to small scales at which it can be dissipated. A major open question in this process is how the energy is finally dissipated at small scales. The Earth's magnetosheath is a typical turbulent environment with in situ spacecraft observations, so it is an ideal laboratory to study this problem. This study analyzes a series of magnetic peak structures in the magnetosheath using Magnetospheric Multiscale data. The interaction of these ion-scale magnetic peaks can generate thin electron current layers where magnetic reconnection can be triggered. Magnetic reconnection is known to convert magnetic energy into plasma kinetic energy in space and astrophysical plasmas. Our study shows that turbulent energy can be dissipated by reconnection in electron-scale current layer, and the formation of these thin current layers is associated with interaction of the magnetic peaks.

## 1. Introduction

Turbulence is ubiquitous in space and astrophysical plasmas, such as planetary magnetosheath and solar wind (Bruno & Carbone, 2013; Sahraoui et al., 2006; Schekochihin et al., 2009). In turbulent plasmas, energy is transferred from the large scale to the kinetic scale at which energy can be dissipated. This energy cascade and dissipation process is thought to play a significant role in plasma heating, such as in the solar corona (Cranmer et al., 2007). However, it is still an unsolved problem as to how the energy is finally dissipated at small scale. Numerical simulations have shown that turbulent cascade can generate numerous coherent structures characterized by intermittency like current sheets (Dong et al., 2018; Karimabadi et al., 2013; Servidio et al., 2009; Wan et al., 2012). These current sheets can extend from ion scale to electron scale and are found to be sites, where energy dissipation and plasma heating happen. Although some statistical results (Chasapis et al., 2018; Stawarz et al., 2019) supported the relation between turbulent dissipation and coherent structures with strong current density, in situ observations are needed to explore the exact

mechanism(s) in this process. Magnetic reconnection is a possible mechanism, and strong current density and energy dissipation have been found at O-lines therein (e.g., H. S. Fu et al., 2017; S. Wang et al., 2020).

The Earth's magnetosheath downstream of the bow shock is a typical turbulent environment and can be measured by Magnetospheric Multiscale (MMS) in an unprecedented high time resolution (Burch et al., 2016), so it is an ideal laboratory to study dissipation in turbulent plasmas. Retino et al. (2007) reported evidence of magnetic reconnection in turbulent magnetosheath using Cluster data and found electron heating in reconnecting current sheet. This kind of dissipation mechanism by reconnection is considered to be important in turbulent dissipation at small scales (Sundkvist et al., 2007). More reconnection events in turbulent magnetosheath have been studied by recent MMS mission (Phan et al., 2018; Voros et al., 2017; Yordanova et al., 2016). The fields, plasma flows, energy dissipation, and resulting electron heating in these reported events all demonstrate the occurrence of reconnection in the magnetosheath. Recently, global hybrid simulations suggest that magnetosheath downstream of the quasi-parallel shock is filled with magnetic flux ropes and current sheets, which were closely related to reconnection and energy dissipation (Karimabadi et al., 2014; Lu, Wang, et al., 2020). An interesting result in the simulations is the numerous magnetic flux ropes formed in the magnetosheath, suggesting that these flux ropes may be an effective indicator of reconnection sites in the turbulent environments. Due to the turbulent state of the plasma in the magnetosheath, the search for flux ropes and current sheets in spacecraft data can be difficult. Multi-spacecraft method has been used to identify flux ropes and reconnection events (e.g., Chen, Fu, Liu, et al., 2019; H. S. Fu et al., 2016) and has been found efficient to study the currents in flux ropes and X-lines statistically (Chen et al., 2018). A bipolar variation of the magnetic field component accompanied with the enhancement of the axial field is the typical observational signature of a flux rope (e.g., Roux et al., 2015; Russell & Elphic, 1978; Zong et al., 2004) in spacecraft data. Yao et al. (2018) suggested that in some cases magnetic bottle like structures, such as the mirror mode structure, can show similar observational features of magnetic field with flux ropes. Individual observations of flux ropes (Chen, Fu, Wang, et al., 2019; S. Y. Huang et al., 2016; Yao, Shi, et al., 2020) and current sheets (Phan et al., 2018; Voros et al., 2017; Yordanova et al., 2016) in the magnetosheath have been reported by MMS, however, simultaneous observation of them has so far been scarce.

In this work, we present observational evidence for the relation between magnetic peaks (MPs), current layers, and energy dissipation in the Earth's magnetosheath using MMS data. We used magnetic field data from the Fluxgate Magnetometer (Russell et al., 2016) with a 128/s sampling rate, electric field data from Electric Double Probes (Ergun et al., 2016; Lindqvist et al., 2016) with a 8,192/s sampling rate, and electrons data with a 30 ms resolution and ions data with a 150 ms resolution from Fast Plasma Investigation (Pollock et al., 2016).

## 2. A Series of MPs in Magnetosheath

Figures 1a–1e show an overview of the MMS observations on November 4, 2015 at 04:34:05–04:36:40 UT. MMS was located at (10.2, 1.9,  $-0.4$ )  $R_E$  in geocentric solar ecliptic (GSE) coordinates, and was in the magnetosheath before 04:36:15 UT, characterized by the dominant low-energy ( $<200$  eV) electron population (Figure 1a) and high plasma density (Figure 1c). After 04:36:15 UT, MMS crossed the bow shock and entered into the solar wind. In this study, we mainly focus on the measurement of the magnetosheath with strong magnetic field fluctuations (Figure 1b). Between 04:34:25 and 04:35:20 UT, these magnetic field fluctuations corresponded to a total of nine MPs in which magnetic field magnitude rapidly increased and then returned to the ambient value. In this interval, ion flows were mainly in the **X** and **Z** directions and the intensity was up to  $200 \text{ km s}^{-1}$  (Figure 1d), suggesting that all the MPs were carried by the high-speed plasma flows.

Between 04:35:00 and 04:35:20 UT, five MPs with intense current density were observed one after another. This interval was enlarged in Figures 1f–1i. The vertical cyan dashed lines represent the peak values of magnetic field magnitude. Then, each of MPs was divided into two parts, the leading and trailing parts. Electron density had a local minimum just at the center, and asymmetries at the two parts of MPs (Figure 1g). Inside three MPs (at  $\sim 04:35:07$ ,  $\sim 04:35:10$ , and  $\sim 04:35:14$  UT) named MP1–MP3, the large current density spikes were always observed in the trailing parts (Figure 1h), with  $|\mathbf{J}| > 2 \mu\text{A m}^{-2}$ . The current density was calculated by the formula  $\mathbf{J} = N_e e (\mathbf{V}_i - \mathbf{V}_e)$  where  $N_e$  is the electron number density,  $e$  is the elementary coulomb charge, and  $\mathbf{V}_i$  and  $\mathbf{V}_e$  are the ion and electron bulk flow velocities. These thin current layers mainly carried

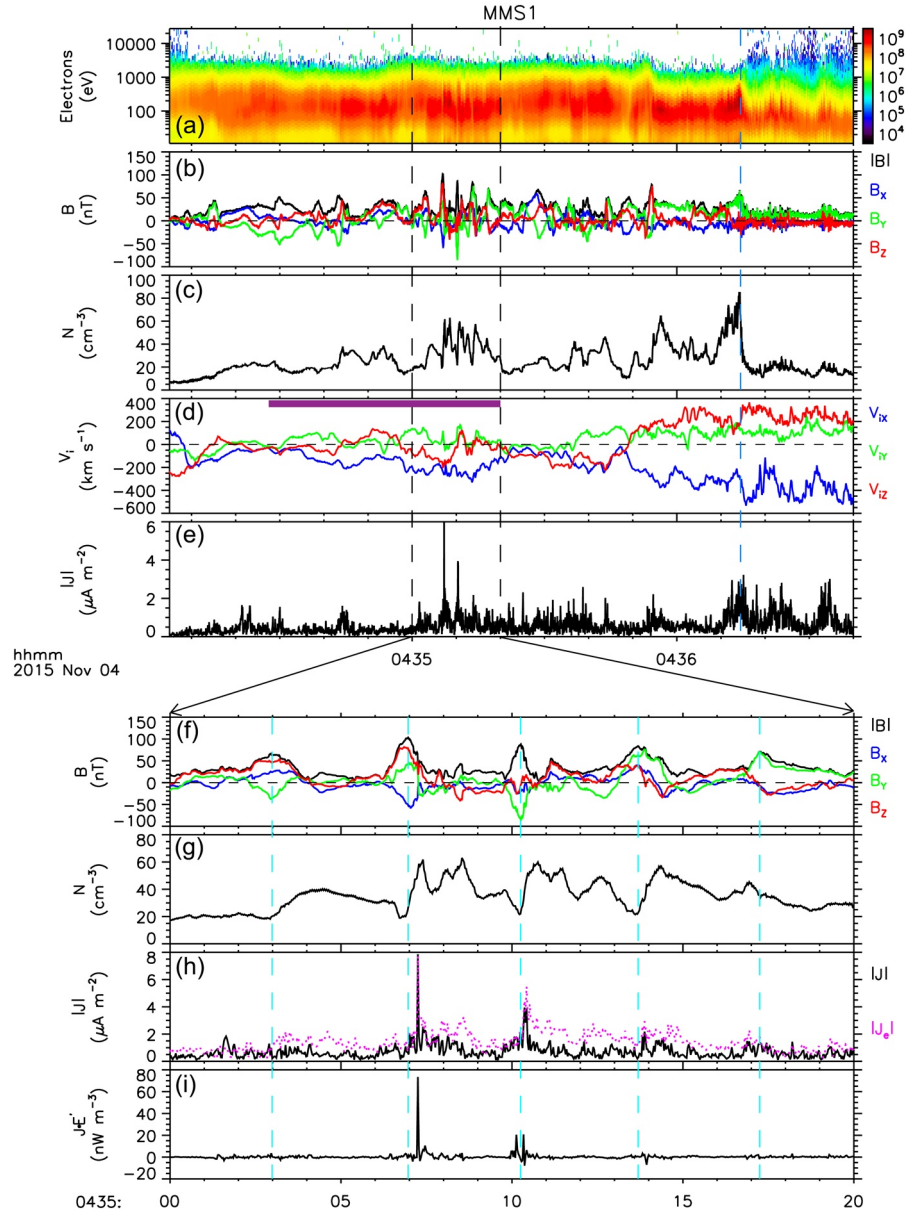


**Figure 1.** Overview of Magnetospheric Multiscale 1 (MMS1) observations. (a) Electron energy-time spectrogram of differential energy fluxes (color scale, in units of  $\text{keV cm}^{-2} \text{s}^{-1} \text{sr}^{-1} \text{keV}^{-1}$ ). (b) Magnetic field. (c) Electron number density. (d) Ion velocity. (e) Current density. (f–i) Enlarged view of observations: (f) Magnetic field, (g) Electron number density, (h) Total (black trace) and electron (magenta trace) current density, (i)  $\mathbf{J} \cdot \mathbf{E}' = \mathbf{J} \cdot (\mathbf{E} + \mathbf{V}_e \times \mathbf{B})$ . All the data are shown in the geocentric solar ecliptic (GSE) coordinates. The interval of magnetosheath high-speed ion jet is denoted by purple bar in panel (d). The vertical cyan dashed lines mark the magnetic field maximum in five magnetic peaks.

by electrons were embedded within the larger-scale current layers, where current density was generally smaller than  $2 \mu\text{A m}^{-2}$ . Figure 1i shows  $\mathbf{J} \cdot \mathbf{E}'$ , where  $\mathbf{E}' = \mathbf{E} + \mathbf{V}_e \times \mathbf{B}$ .  $\mathbf{J} \cdot \mathbf{E}'$  is the energy conversion from electromagnetic field to plasmas in the electron rest frame (e.g., Zenitani et al., 2011). Strong energy conversion was observed inside current density spikes.

### 2.1. MPs with Intense Electric Current

Figures 2a–2h display detailed fields and plasma observations for MP1–MP3 in GSE coordinates. Three MPs were marked with purple shadows. Their propagation velocity were estimated to be  $184.1 \text{ km s}^{-1}$  along  $\mathbf{n}_1 = (-0.88, -0.14, -0.45)$  for MP1,  $207.9 \text{ km s}^{-1}$  along  $\mathbf{n}_2 = (-0.94, 0.14, 0.31)$  for MP2, and  $208.8 \text{ km s}^{-1}$

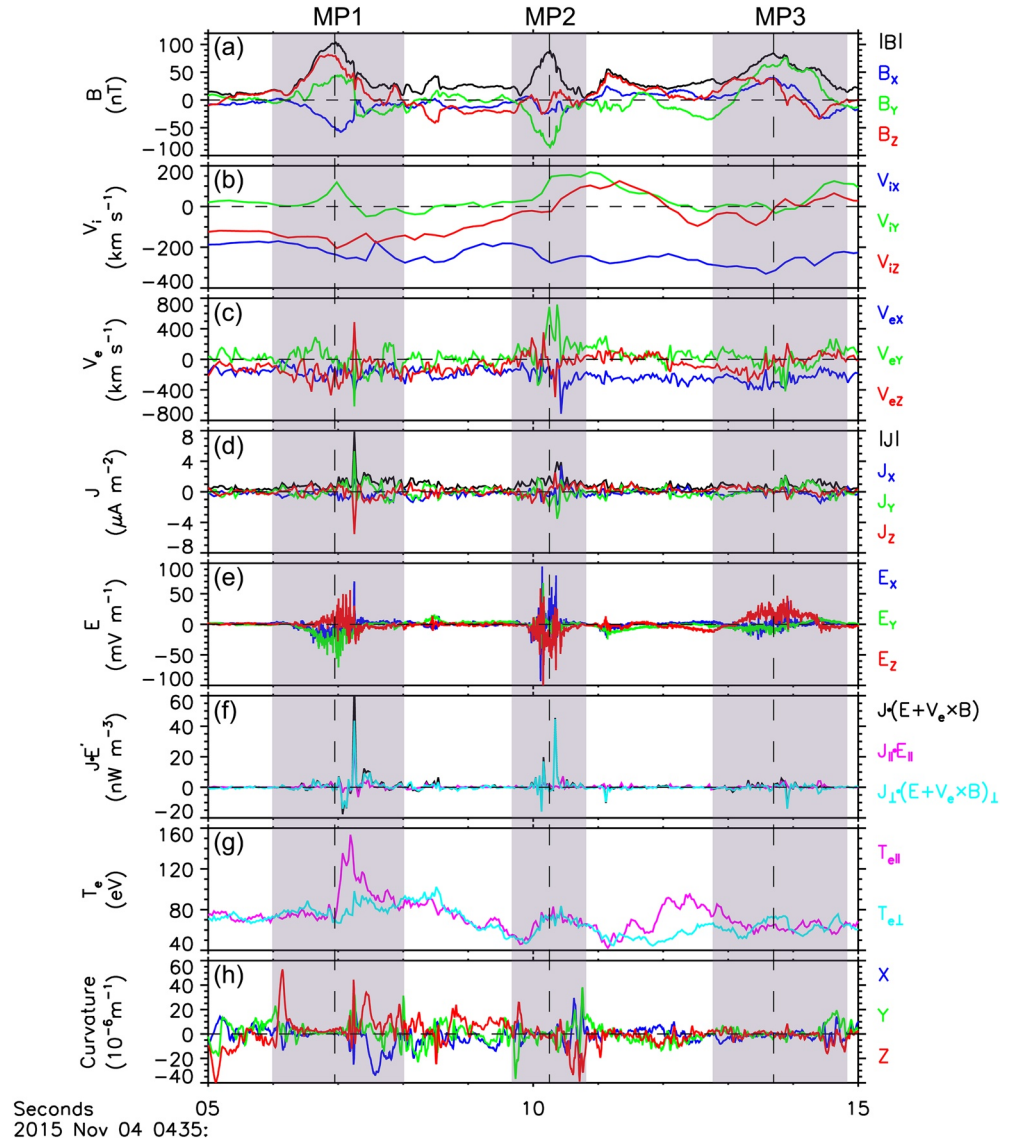


**Figure 2.** Detailed Magnetospheric Multiscale 1 (MMS1) observations of three magnetic peaks. (a) Magnetic field. (b) Ion velocity. (c) Electron velocity. (d) Current density. (e) Electric field. (f)  $\mathbf{J} \cdot \mathbf{E}' = \mathbf{J} \cdot (\mathbf{E} + \mathbf{V}_e \times \mathbf{B})$ . (g) Parallel and perpendicular electron temperature. (h) Magnetic field line curvature. All the data are shown in the geocentric solar ecliptic (GSE) coordinates. Purple shaded region represent three magnetic peaks, named MP1–MP3, respectively. The vertical dashed lines mark the magnetic field maximum in MP1–MP3. MP, magnetic peak.

along  $\mathbf{n}_3 = (-0.91, 0.01, 0.43)$  for MP3, respectively, by the timing method (Schwartz, 1998). Correspondingly, the cross sections through three MPs were 368.2 km ( $\sim 7.2 d_i$ ), 207.9 km ( $\sim 4.1 d_i$ ), and 417.6 km ( $\sim 8.2 d_i$ ), respectively. Here,  $d_i$  was the ion inertial length and was calculated to be 51.0 km by using density minimum of  $20 \text{ cm}^{-3}$  in MPs.

Inside three MPs, some similar features have been observed. For example, bipolar magnetic field variation in one direction with an enhancement in another direction can be found therein (Figure 2a) indicating a helical magnetic topology of flux rope. The current density showed a double-layered structure characterized by the large-scale current layer and an embedded thin electron current layer (Figure 2d), which was rarely reported in magnetosheath MPs. Given that electric field had a large amplitude (Figure 2e), strong positive  $\mathbf{J} \cdot \mathbf{E}' = \mathbf{J} \cdot (\mathbf{E} + \mathbf{V}_e \times \mathbf{B})$  was evident inside these embedded thin current layers (Figure 2f). Positive  $\mathbf{J} \cdot \mathbf{E}'$  implied that magnetic energy was converted into the plasma kinetic energy here.

Specifically, in the trailing part of MP1 (04:35:07.2–04:35:07.3 UT), an abrupt reversal of  $B_y$  from positive to negative was observed. However, this reversal point was not at the MP1 center where the magnetic field magnitude had a maximum. Ion flows  $V_{ix}$  were larger in the trailing part of MP1 (Figure 2b), possibly implying a contraction of the structure, while electron flows had a large spike at the  $B_y$  reversal point ( $\sim$ 04:35:07.25 UT, Figure 2c). Due to the strong electron flows, a thin current layer ( $|\mathbf{J}| \sim 8 \mu\text{A m}^{-2}$ , Figure 2d) was observed at the point and mainly carried by the electrons. Figure 2g plots the parallel and perpendicular electron temperatures. In the trailing part of MP1, electrons were significantly heated in both the parallel and perpendicular directions, with a much higher parallel temperature. Figure 2h plots the curvature vector of magnetic field lines ( $\mathbf{b} \cdot \nabla \mathbf{b}$ , where  $\mathbf{b}$  is magnetic field unit vector) calculated by the magnetic field measurements at four MMS satellites. The curvature of one magnetic field line reflects the direction of its curving. At the leading edge of the MP1 (before 04:35:06.3 UT), magnetic curvature vector was dominated in the  $\mathbf{Z}$  direction while at the trailing edge (04:35:07.4–04:35:07.9 UT), magnetic curvatures were mainly in both the  $\mathbf{Z}$  and  $\mathbf{X}$  directions. It should be noted that the curvature vector in  $\mathbf{Z}$  direction did not change sign at the two edges as expected. The reason was presented later. In addition to the large curvature in the two edges, the curvature was also large inside thin current layer at 04:35:07.25 UT.

Despite the similarities between MP1 and MP2 as mentioned above, more differences in MP2 should be noted. First, the reversed magnetic field component was  $B_z$ , not as that in MP1. Additionally,  $B_z$  changed sign just at the peak of the magnetic field magnitude, rather than in thin current layer ( $\sim$ 04:35:10.4 UT). In MP2, electrons were significantly heated equally between the parallel and perpendicular directions, different from that in MP1, where the parallel temperature was much higher than the perpendicular temperature. Another significant difference is that the magnetic field curvatures reversed in both  $\mathbf{Y}$  and  $\mathbf{Z}$  directions in MP2 indicating a helical field configuration. The magnetic field curvatures reversed from  $-\mathbf{Y}$  to  $+\mathbf{Y}$  and reversed from  $+\mathbf{Z}$  to  $-\mathbf{Z}$ . In addition, the components of curvature vector were small in the inner part of MP2 suggesting that the magnetic field lines become straighter. This feature of curvature variation is similar to that in previous studies about flux ropes (e.g., Shen et al., 2007; Sun et al., 2019; Yang et al., 2014).

In MP3 thin current layer ( $\sim$ 04:35:13.9 UT), current density was only about  $2 \mu\text{A m}^{-2}$ , just slightly larger than surrounding current density. Electric fields had a dominant  $E_z$  component, which had a nearly symmetric distribution. Additionally, energy conversion was much smaller compared with that in MP1–MP2. Parallel electron temperature had a dip at the center, while perpendicular temperature undulated inside the MP3. Magnetic field curvatures reversed in both  $\mathbf{X}$  and  $\mathbf{Z}$  directions, and a large curvature in  $\mathbf{Y}$  direction can be seen at the trailing edge. As a whole, MP3 had weaker variations in terms of field and current, not as that in MP1–MP2.

## 2.2. MPs with Signature of Magnetic Flux Rope

It is challenging to distinguish the magnetic flux rope from the magnetic bottle-like structure. If the spacecraft crossed a magnetic flux rope or magnetic bottle-like structure in the plane perpendicular to the axis, the same magnetic field signatures were detected, that is, bipolar magnetic field variation and enhanced axial field. A significant difference between these two structures is the angle between the magnetic field and the spacecraft trajectory close to the structure center (Yao et al., 2018). Specifically, this angle is equal to  $0^\circ$  or  $180^\circ$  for the flux ropes, and is equal to  $90^\circ$  for the magnetic bottle like structures (Figure 4 in Yao et al., 2018). Figure 3 shows this angle for MP1–MP3 in their own LMN coordinates with the magnetic field magnitude, components and curvatures as well, in which  $\mathbf{L}$  is along the axes of the MPs.

Between 04:35:06.2 and 04:35:07.2 UT (Figures 3a–3c, before vertical dashed line), MP1 had clear bipolar  $B_M$  and  $B_N$  from positive to negative and a strong axial field  $B_L$  at the reversal point (Figure 3a). This polarity change in  $B_M$  and  $B_N$  cannot be revealed in GSE coordinates (Figure 2a). At the  $B_M$  reversal point ( $\sim$ 04:35:06.9 UT), the angle  $\theta_{BV}$  between the magnetic field and the spacecraft trajectory in the MN plane changed from  $0^\circ$  to  $180^\circ$  quickly (Figure 3b), implying that it is a flux rope. The velocity of MP1 in the satellite frame was calculated by the timing method, then the spacecraft velocity can be obtained if we assume that the MP1 does not move. The spacecraft trajectory is determined by the spacecraft velocity and magnetic field variations. An illustration is given in Figure 3d. After 04:35:07.2 UT, another bipolar  $B_M$  from negative to positive was observed, accompanied with the decrease of  $B_L$  and  $|\mathbf{B}|$ . At this new reversal point, a thin electron current layer was formed. At the leading edge (04:35:06.0–04:35:06.3 UT) and trailing edge

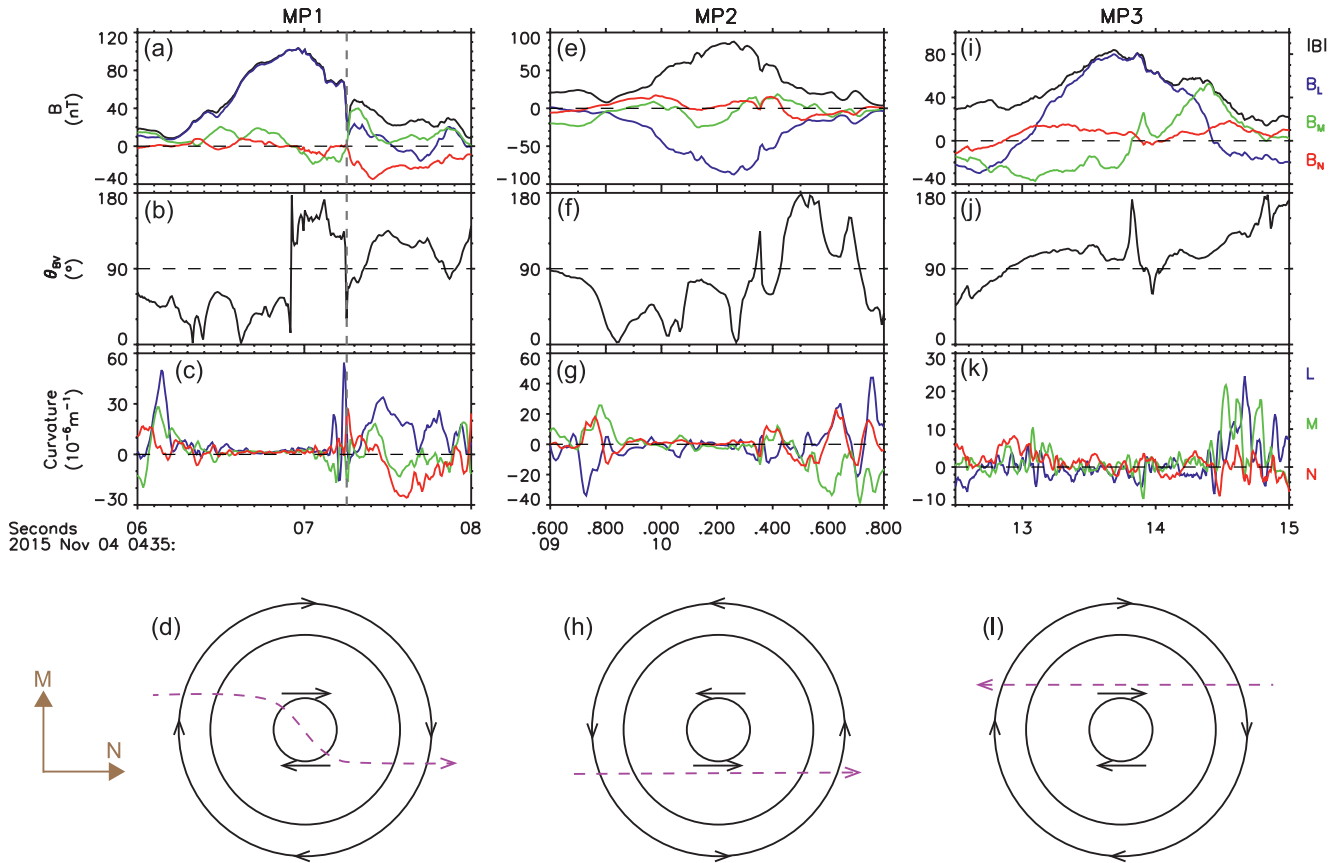


**Figure 3.** Observational signatures of flux ropes. (a) Magnetic field magnitude and components from Magnetospheric Multiscale 1 (MMS1) in the LMN coordinates. (b) Angle  $\theta_{BV}$  between the field line and the spacecraft trajectory in MN plane. (c) Magnetic field line curvature in the LMN coordinates. (d) Schematic of the spacecraft trajectory in the MN plane for MP1. Black lines with arrows represent the magnetic field lines. Magenta dashed line with an arrow denotes a possible MMS trajectory. (e–h), (i–l) The data are displayed in the same format for MP2 and MP3. The data for three magnetic peaks are shown in their own LMN coordinates. For MP1,  $\mathbf{L} = (-0.48, 0.40, 0.78)$ ,  $\mathbf{M} = (0.48, -0.62, 0.62)$ ,  $\mathbf{N} = (0.73, 0.67, 0.10)$ . For MP2,  $\mathbf{L} = (0.32, 0.95, 0.00)$ ,  $\mathbf{M} = (0.00, 0.00, 1.00)$ ,  $\mathbf{N} = (0.95, -0.32, 0.00)$ . For MP3,  $\mathbf{L} = (0.43, 0.89, 0.18)$ ,  $\mathbf{M} = (-0.46, 0.38, -0.80)$ ,  $\mathbf{N} = (-0.78, 0.26, 0.58)$ . MP, magnetic peak.

(04:35:07.5–04:35:07.9 UT) of MP1, the curvatures reversed in  $\mathbf{N}$  direction. This feature of magnetic curvature cannot be found in GSE coordinates.

In MP2, only one bipolar  $B_M$  from negative to positive can be observed (Figure 3e). Figure 3f shows that the angle  $\theta_{BV}$  is nearly  $0^\circ$  at the center of the MP2, implying that it is a flux rope. Magnetic curvatures reversed in  $\mathbf{L}$  and  $\mathbf{M}$  directions (Figure 3g), supporting that MP2 had a helical field configuration. In MP3, magnetic field signals (Figures 3i and 3k) and the angle  $\theta_{BV}$  (Figure 3j) also demonstrate that it is a flux rope.

### 3. Magnetic Reconnection in the Thin Current Layer

To examine whether the reconnection was ongoing inside thin current layer at  $\sim 04:35:07.25$  UT in MP1, MMS data were transferred into the current sheet boundary normal (LMN) coordinates. Here, we determined the LMN coordinates as follows:  $\mathbf{M} = (\mathbf{B}_1 \times \mathbf{B}_2) \times (\mathbf{B}_1 - \mathbf{B}_2) / |(\mathbf{B}_1 \times \mathbf{B}_2) \times (\mathbf{B}_1 - \mathbf{B}_2)|$ ,  $\mathbf{N} = (\mathbf{B}_1 \times \mathbf{B}_2) / |\mathbf{B}_1 \times \mathbf{B}_2|$ , and  $\mathbf{L} = \mathbf{M} \times \mathbf{N}$ , where  $\mathbf{B}_1 = (-37.7, 35.0, 41.0)$  (nT) and  $\mathbf{B}_2 = (-3.3, -27.4, 39.0)$  (nT) are average magnetic field at the two edges of current layer. Figures 4a–4g show observations of this current layer in LMN coordinates. The thickness of it was estimated to be 11.8 km ( $\sim 0.23 d_i$ ). Inside it,  $B_L$  reversed from positive ( $\sim 50$  nT) to negative ( $\sim -20$  nT) in 0.06 s (Figure 4a), consistent with an intense and electron-scale out-of-plane current  $J_M$  (Figure 4c). The guide field  $B_M$  was strong ( $\sim 40$  nT), almost comparable to the reconnecting field  $B_L$ . At the reversal point of  $B_L$ , a negative enhancement in  $V_{eL}$  was about  $450 \text{ km s}^{-1}$  compared to background flow (Figure 4b), which was larger than local ion Alfvén speed ( $200 \text{ km s}^{-1}$ ). Meanwhile, Hall electric field

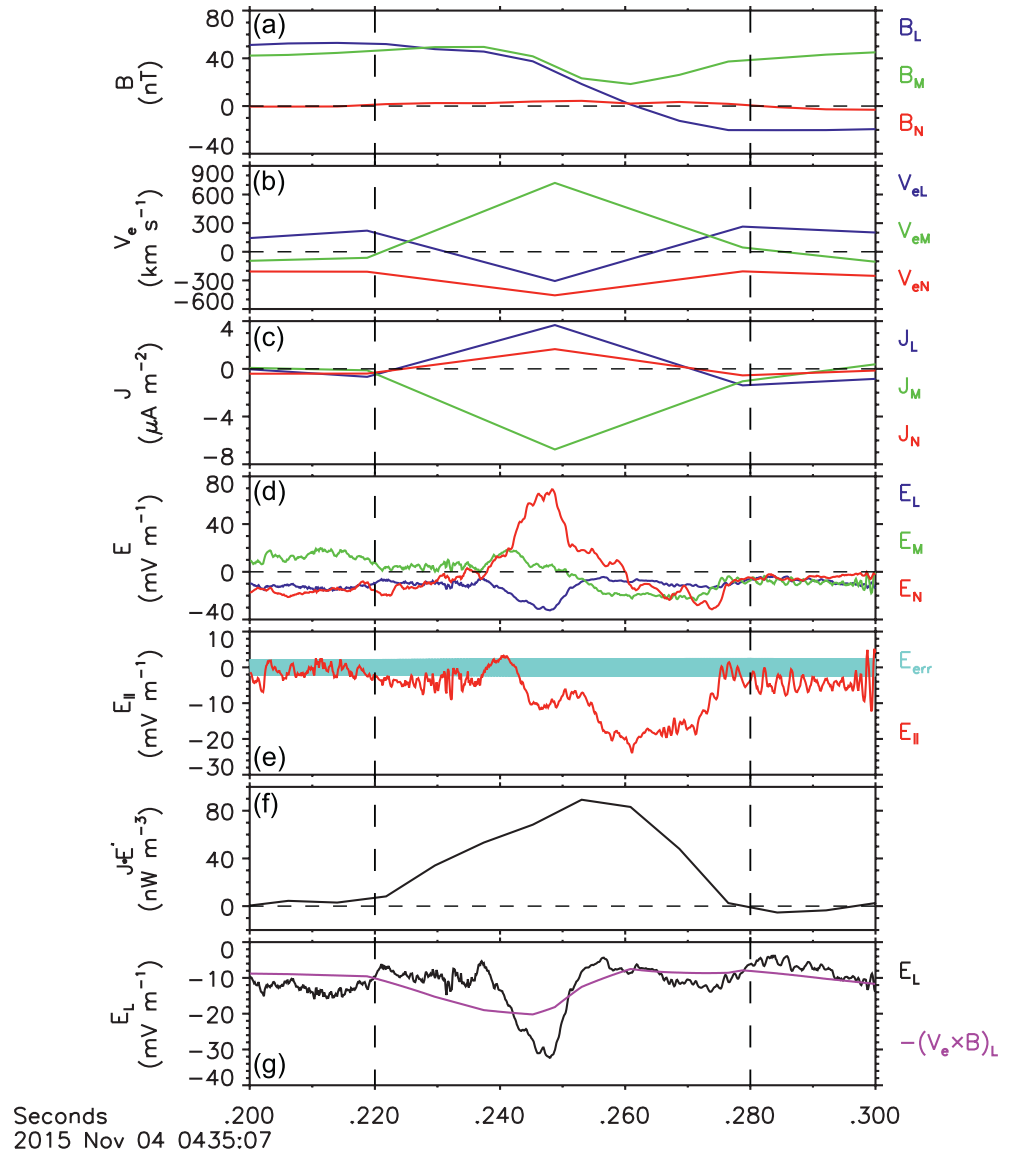


**Figure 4.** Direct evidence of magnetic reconnection in thin current layer. (a) Magnetic field. (b) Electron velocity. (c) Current density. (d) Electric field. (e) Parallel electric field with uncertainty in cyan. (f)  $\mathbf{J} \cdot \mathbf{E}' = \mathbf{J} \cdot (\mathbf{E} + \mathbf{V}_e \times \mathbf{B})$ . (g) Electric field component  $E_L$  and  $-(\mathbf{V}_e \times \mathbf{B})_L$ . All the data are from Magnetospheric Multiscale 1 (MMS1) and are shown in the LMN coordinates.

$E_N$  showed an asymmetric bipolar variation (Figure 4d). Remarkably, a unipolar parallel electric field  $E_{||}$  with amplitude up to  $-20 \text{ mV m}^{-1}$  was observed across the current layer (Figure 4e). This intense  $E_{||}$  was rare even in guide field reconnection, and may be important for electron acceleration. In Figure 4g, there was significant deviation in the observed  $E_L$  and  $-(\mathbf{V}_e \times \mathbf{B})_L$  (similar deviations also existed in  $\mathbf{M}$  and  $\mathbf{N}$  directions) implying that electrons were not frozen-in. Furthermore, energy conversion  $\mathbf{J} \cdot \mathbf{E}'$  was positive indicating that magnetic energy was converted into kinetic energy (Figure 4f). Based on the observations of super-Alfvén electron outflow jets, Hall electric fields, non-frozen-in electrons, and magnetic-to-particle energy conversion inside a current layer, it is concluded that reconnection was occurring. This reconnection event was first reported by Wilder et al. (2018), and we analyzed this event here using a new LMN coordinates. We note that in MP2 thin current layer where  $\mathbf{J} \cdot \mathbf{E}'$  was about  $40 \text{ nW m}^{-3}$ , a partial crossing of reconnecting current sheet was detected indicated by a unipolar Hall electric field. In MP3, no reconnection signatures were observed, and energy dissipation was smaller than that in MP1–MP2.

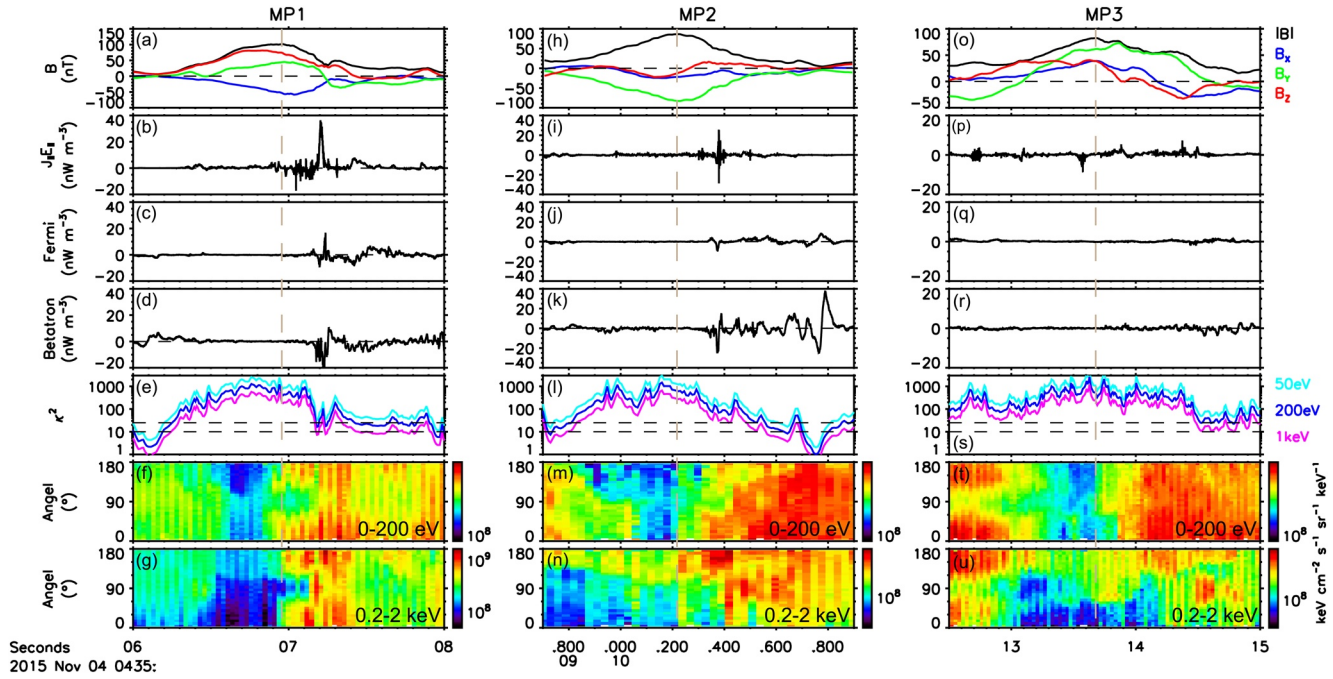


**Figure 5.** Electron heating in three magnetic peaks. (a) Magnetic field magnitude and components at the barycenter of four Magnetospheric Multiscale (MMS) satellites. (b–d) Electron energy gain rate by parallel electric field, Fermi and betatron acceleration, respectively. (e) Adiabatic parameter  $\kappa^2$  for electrons with energy of 50, 200, and 1,000 eV, respectively.  $\kappa^2$  is defined as the ratio between the local magnetic field curvature radius and the electron's Larmor radius. (f, g) Electron pitch angle distributions in energy range 0–200 eV and 0.2–2 keV, respectively, from MMS3. Panels (h–n) and (o–u) are in the same format as panels (a–g). The vertical dashed lines mark the magnetic field maximum in MP1–MP3. MP, magnetic peak.

#### 4. Electron Heating in MPs

As shown in Figure 2g, electrons were heated in both the parallel and perpendicular directions inside MP1–MP3. To study electron behavior, we plotted electron pitch angle distributions (ePAD) in different two energy bands (0–200 eV and 0.2–2 keV) in Figures 5f, 5g, 5m, 5n, 5t, and 5u, for MP1–MP3. These two energy bands correspond to magnetosheath and heated electron populations, respectively (e.g., Pu et al., 2013; J. Zhong et al., 2013).

In MP1, the ePAD were drastically different on the two parts. In the leading part, parallel fluxes of magnetosheath electrons were higher than antiparallel fluxes (Figure 5f), while heated electrons had higher fluxes in the antiparallel direction (Figure 5g). In addition, both two electron populations had lower fluxes in the leading part, consistent with a lower electron density (Figure 1g). In the trailing part, both two electron populations were observed simultaneously in parallel and antiparallel directions. Inside MP2 and MP3, the ePAD showed some differences from those in MP1. First, the ePAD showed fewer differences between leading and trailing parts, especially for MP3. Second, there were more fluxes in the antiparallel direction in both the leading and trailing parts (Figures 5n and 5u). The fluxes in the parallel direction were much lower. Third, there were increase of the perpendicular fluxes in some local regions of trailing parts (Figures 5n and 5u).

To study the electron heating in the MPs, we calculated the electron energy gain rate by different mechanisms using the following expression (Dahlin et al., 2014):

$$\frac{dU}{dt} = J_{\parallel} E_{\parallel} + \frac{p_{\perp}}{B} \left( \frac{\partial B}{\partial t} + \mathbf{u}_{\mathbf{E}} \cdot \nabla B \right) + \left( p_{\parallel} + nm_e u_{\parallel}^2 \right) \mathbf{u}_{\mathbf{E}} \cdot \mathbf{k}, \quad (1)$$

where  $\mathbf{u}_{\mathbf{E}}$  is the “ $\mathbf{E} \times \mathbf{B}$ ” drift velocity,  $\mathbf{k} = \mathbf{b} \cdot \nabla \mathbf{b}$  is the curvature,  $u_{\parallel}$  is the parallel bulk velocity,  $n$  is the electron density, and  $p_{\perp}$  and  $p_{\parallel}$  are the perpendicular and parallel pressures, respectively. The first term in

Equation 1 is the acceleration due to the parallel electric field. The second term represents betatron acceleration in perpendicular direction, and the last term is Fermi acceleration in parallel direction. Equation 1 is derived based on the guiding-center approximation and neglects nonadiabatic acceleration mechanisms and electron scattering. To determine the intensity of electron dissipation, an adiabatic parameter  $\kappa^2$  at different energies was calculated. This adiabatic parameter has been used to study the scattering in the reconnection diffusion region and outflow region (e.g., Eriksson et al., 2020; Lavraud et al., 2016).  $\kappa^2$  is defined as the ratio between the local magnetic field curvature radius and the electron's Larmor radius (Büchner & Zelenyi, 1989). Theory predicts that electron scattering is efficient and electron motion is possibly nonadiabatic, when  $\kappa$  is close to 1 (Büchner & Zelenyi, 1989). In this case, Equation 1 would be inappropriate to calculate the electron energy gain rate.

Electrons can be accelerated by parallel electric field directly in the field-aligned direction (Egedal et al., 2012; R. Wang et al., 2014). Another important mechanism for parallel heating is through Fermi reflection from contracting magnetic field lines (Drake et al., 2006; X. R. Fu et al., 2006). In this process, electrons gain energy by the curvature drift along the inductive electric field. Analogously, magnetic gradient drift can drive electron heating in the perpendicular direction by betatron acceleration, which is often found in the jet front (H. S. Fu et al., 2011; Wu et al., 2013). Previous simulations have studied the role of parallel electric field, Fermi and betatron acceleration in electron heating (Dahlin et al., 2014; Wang, Lu, Huang, 2016).

Figures 5b–5d show the electron energy gain rate by three mechanisms in MP1. Parallel electric field acceleration had a large peak ( $\sim 40 \text{ nW m}^{-3}$ ) in the reconnecting current layer ( $\sim 04:35:07.2 \text{ UT}$ , Figure 5b), consistent with a unipolar negative  $E_{\parallel}$  in Figure 4e, which can accelerate electrons along magnetic field lines (Figures 5f and 5g). On the left side of this current layer ( $04:35:07.0\text{--}04:35:07.2 \text{ UT}$ ),  $J_{\parallel}E_{\parallel}$  fluctuated dramatically and electron parallel temperature had an obvious increase therein (Figure 2g). Near the peak of  $J_{\parallel}E_{\parallel}$ , the Fermi acceleration also had a positive peak with amplitude exceeding  $10 \text{ nW m}^{-3}$  (Figure 5c) consistent with the enhanced fluxes in field-aligned direction (Figures 5f and 5g). The betatron acceleration had a negative-positive variation inside thin current layer with a higher negative acceleration rate (Figure 5d). On average, the betatron acceleration is negative in the current layer. Therefore, the parallel electric field acceleration is the dominant acceleration mechanism in the reconnecting current layer of MP1 with a small contribution from Fermi acceleration. Three acceleration rates were all nearly zero in the leading part of MP1. Note that three acceleration rates were calculated at the barycenter of four MMS satellites, while the ePAD were plotted using data from MMS3 which is the closest satellite to the center of MMS tetrahedron. Figure 5e plots the  $\kappa^2$  for electrons with energy of 50, 200, and 1,000 eV, respectively. For the electrons with low energy (50 eV, cyan line in Figure 5e) corresponding to that shown in the ePAD spectrogram of Figure 5f, the value of  $\kappa^2$  was large ( $>25$ ) throughout the MP1 and had a minimum in the current layer. So these low-energy electrons were adiabatic in MP1 and their acceleration can be estimated by Equation 1. For the electrons with the higher energy, the value of  $\kappa^2$  approached 25 (200 eV, blue line in Figure 5e) and was even down to 10 (1 keV, magenta line in Figure 5e) inside the current layer, implying that these electrons were nonadiabatic and could be scattered effectively. This pitch angle scattering can also be revealed in the ePAD spectrogram of Figure 5g which shows that at  $\sim 04:35:07.2 \text{ UT}$ , the field-aligned fluxes of electrons decreased, while perpendicular fluxes had an obvious enhancement. The electron scattering may also explain the local increase of the perpendicular temperature and decrease of the parallel temperature. This result is consistent with recent MMS observations about electron scattering in the X-line and outflow region (e.g., Eriksson et al., 2020; Lavraud et al., 2016).

Figures 5i–5k show the electron energy gain rates in MP2. Parallel electric field acceleration rate (Figure 5i) fluctuated with largest amplitudes in the thin current layer ( $\sim 04:35:10.4 \text{ UT}$ ), but overall the net acceleration rate was about zero. Positive Fermi acceleration rates (Figure 5j) were observed in the trailing part ( $04:35:10.5\text{--}04:35:10.7 \text{ UT}$ , not in the thin current layer), with a peak value around  $5 \text{ nW m}^{-3}$ . Correspondingly, the fluxes of the heated electrons were enhanced along the antiparallel direction (Figure 5n). The betatron acceleration rate (Figure 5k) showed positive and negative variations in the trailing part ( $04:35:10.5\text{--}04:35:10.7 \text{ UT}$ ) with a peak value around  $10 \text{ nW m}^{-3}$ , except a large value of  $40 \text{ nW m}^{-3}$  at  $\sim 04:35:10.8 \text{ UT}$ . On average, the betatron acceleration rate had a net positive effect in the trailing part. Therefore, in MP2, electrons were mainly heated in the trailing part by Fermi and betatron mechanisms. Due to the comparable peak values of Fermi and betatron acceleration rates, electrons were heated both in parallel and perpendicu-

lar directions. Therefore, a nearly equal heating in the parallel and perpendicular directions can be observed in MP2 (Figure 2g). The  $\kappa^2$  was found to have several local increase in the trailing part suggesting that electrons were locally adiabatic and their acceleration can be estimated by Equation 1.

Figures 5p–5r show the electron energy gain rates in MP3. Although three acceleration rates were all much smaller compared with those in MP1 and MP2, the Fermi and betatron acceleration rates were still dominant acceleration mechanisms in the trailing part of MP3 (Figures 5q and 5r). The  $\kappa^2$  was above 25 in most of the MP3 except in a small region (04:35:14.5–04:35:14.9 UT). It suggests that in MP3, Equation 1 is valid for the dominant electron populations with energy smaller than 1 keV.

## 5. Discussion and Conclusions

Using MMS data in Earth's magnetosheath, we studied energy dissipation and electron heating in turbulent coherent structures. A series of MPs characterized by the enhancements of magnetic field magnitude was detected downstream of the bow shock. MPs are common magnetic structures observed in the magnetosheath and can be classified into two types: flux ropes (e.g., S. Y. Huang et al., 2016; Wang et al., 2019) and mirror mode peaks (e.g., Yao et al., 2018). Yao et al. (2018) proposed that the angle between the field line and the spacecraft trajectory can be used to distinguish these two structures. The MPs in our events were identified as flux ropes based on this method. We noted that the MPs were characterized by the strong axial fields which were nearly equal to the magnetic field magnitudes near the MPs center. A strong core field accompanied with the bipolar variation of the magnetic field is considered to be the typical signature of a helical flux rope (Zong et al., 2004). The reversed magnetic curvatures in MPs also support the helical field configurations of flux ropes. In addition, the curvatures were small in the inner regions of MPs suggesting that the core magnetic field lines become straighter. Similar curvature variations have also been reported in magnetotail flux ropes (e.g., Sun et al., 2019; Yang et al., 2014).

Inside MPs, a striking feature is an extremely thin electron current layer embedded within a much broader ion-scale current layer. This double-layered current structure is rarely reported in magnetosheath MPs and their formation will be discussed later. Inside the thinnest electron current layer ( $\sim 0.23 d_i$ ), super-Alfvén electron outflow jets, Hall electric fields, non-frozen-in electrons, and magnetic-to-particle energy conversion were observed simultaneously indicating that reconnection was occurring. These observations reveal a close relation between MPs, current layers and magnetic reconnection in turbulent magnetosheath, consistent with simulation results (Karimabadi et al., 2014; Lu, Wang, et al., 2020). More observation results are needed to reveal a statistical connection between MPs and current layers.

An important question is how the electron-scale current layer was formed in MP1. A reasonable speculation is that MP1 were formed by coalescence of two smaller MPs. Such a scenario is supported by simulations (e.g., Oka et al., 2010), and has been observed in the magnetotail (Wang, Lu, Nakamura, et al., 2016; Zhao et al., 2016) and at the magnetopause (R. Wang et al., 2017; Zhou et al., 2017). However, in the magnetosheath, relevant observations were rare probably due to variable flows, different from that in the magnetotail (mainly in the  $\mathbf{X}_{\text{GSE}}$  direction) and at the magnetopause (mainly in the  $\mathbf{Z}_{\text{GSE}}$  direction). We note that MP1 was carried by the high-speed earthward flows, and  $V_{ix}$  in the trailing part was larger than that in the leading part. This suggests that electron-scale current layer may result from the interaction of two neighboring MPs pushed together by the ion flows in which they were embedded. Strong core field and plasma density dip at the MP1 center are in good agreement with the simulation results of merged flux ropes (Zhou et al., 2014). Different ePAD on the two sides of MP1 also support this speculation, as the leading and trailing parts were not magnetically connected and may be two originally separated MPs. Similar observations of ePAD in flux ropes have been reported at the magnetopause (Fargette et al., 2020; Kacem et al., 2018; Øieroset et al., 2019) and were interpreted as the interaction of two distinct flux tubes. Contrarily, in MP3, the intensity of thin current sheet and energy dissipation were both much smaller, and no reconnection signatures were seen here. It is unclear whether the differences between MP1 and MP3 are the temporal evolution of the coalescence process or due to the spacecraft trajectory through them.

In three MPs, electrons were significantly heated in both the parallel and perpendicular directions, thus the electron energy gain rates by parallel electric field, Fermi and betatron acceleration were calculated quantitatively. These three mechanisms have been found successful in explaining electron heating during recon-

nection (Dahlin et al., 2014; Q. M. Lu et al., 2018; Wang, Lu, Huang, et al., 2016) and have been employed to study the accelerations in magnetotail flux ropes (Z. H. Zhong et al., 2020). The simulations suggested that flux ropes can accelerate electrons effectively in turbulent magnetic reconnection (e.g., S. Lu et al., 2019; Lu, Artemyev, et al., 2020). In our work, we found two main results about electron heating in magnetosheath MPs. First, in reconnecting current layer, where magnetic energy was largely dissipated, acceleration by parallel electric fields is the dominant driver for low-energy electron heating, consistent with the simulation results of acceleration in large guide field reconnection (Dahlin et al., 2014; Wang, Lu, Huang, et al., 2016). In addition, in this region, electrons with high energy (>200 eV) were nonadiabatic and can be scattered effectively. We noted that the field-aligned electrons were scattered to the perpendicular direction, causing a local increase of the perpendicular temperature. Another electron heating process occurred in the trailing edges of the MPs, where electrons were mainly heated by Fermi (Drake et al., 2006; X. R. Fu et al., 2006) and betatron (H. S. Fu et al., 2011; C. Huang et al., 2015) mechanisms. This was probably caused by the converging ion jets in the MPs which were larger in the trailing edges of MPs. Converging jets can cause the magnetic field contraction and compression (Yao, Hamrin, et al., 2020; Z.H. Zhong et al., 2020) and produce high-energy electrons in the field-aligned and perpendicular directions (S. Wang et al., 2019; Z. H. Zhong et al., 2020). Therefore, in our studies, electrons were mainly heated in two regions of MPs, that is, reconnecting current layer and trailing edges of MPs, in different mechanisms.

In conclusion, we presented the observational evidence of energy dissipation within the ion-scale coherent structures in the form of MPs. Three MPs with intense current density were studied in detail. In each of these three MPs, a thin electron current layer was embedded within a broader ion-scale current layer, and was located in the trailing part. Inside one of the thin current layers, direct evidence for reconnection was observed. Electrons were significantly heated in two regions of MPs: reconnecting current layer and trailing edges. All these observations indicate that the ion-scale MPs are coherent structures associated with energy dissipation and electron heating in the magnetosheath. Our studies suggest the relation between MPs, current layers and magnetic reconnection in the magnetosheath, and a scenario of MPs coalescence in good agreement with observational characteristics is proposed to explain this relation.

### Data Availability Statement

All the MMS data used in this work are publicly available from the MMS Science Data Center (<https://lasp.colorado.edu/mms/sdc/public/>).

### Acknowledgments

The authors thank the entire MMS team and instrument principal investigators for providing data. This work is supported by the B-type Strategic Priority Program of the Chinese Academy of Sciences (XDB41000000), the National Natural Science Foundation of China (NSFC) grants (41674143, 41922030, and 41527804), the key research program of frontier sciences CAS (QYZDJ-SSW-DQC010), and the Fundamental Research Funds for the Central Universities.

### References

- Büchner, J., & Zelenyi, L. M. (1989). Regular and chaotic charged particle motion in magnetotail like field reversals: 1. Basic theory of trapped motion. *Journal of Geophysical Research*, *94*, 11821–11842. <https://doi.org/10.1029/ja094ia09p11821>
- Bruno, R., & Carbone, V. (2013). The solar wind as a turbulence laboratory. *Living Reviews in Solar Physics*, *10*, 2. <https://doi.org/10.12942/lrsp-2013-2>
- Burch, J. L., Moore, T. E., Torbert, R. B., & Giles, B. L. (2016). Magnetospheric multiscale overview and science objectives. *Space Science Reviews*, *199*, 5–21. [https://doi.org/10.1007/978-94-024-0861-4\\_2](https://doi.org/10.1007/978-94-024-0861-4_2)
- Chasapis, A., Matthaeus, W. H., Parashar, T. N., Wan, M., Haggerty, C. C., Pollock, C. J., Giles, B. L., et al. (2018). In situ observation of intermittent dissipation at kinetic scales in the Earth's magnetosheath. *The Astrophysical Journal*, *856*, L19. <https://doi.org/10.3847/2041-8213/aaadf8>
- Chen, X. H., Fu, H. S., Liu, C. M., Cao, D., Wang, Z., Dunlop, M. W., et al. (2018). Magnetic nulls in the reconnection driven by turbulence. *The Astrophysical Journal*, *852*, 17. <https://doi.org/10.3847/1538-4357/aa9991>
- Chen, Z., Fu, H., Liu, C. M., Wang, T. Y., Ergun, R. E., Cozzani, G., et al. (2019). Electron-driven dissipation in a tailward flow burst. *Geophysical Research Letters*, *46*, 5698–5706. <https://doi.org/10.1029/2019gl082503>
- Chen, Z., Fu, H., Wang, T., Cao, D., Peng, F., Yang, J., & Xu, Y. (2019). Reconstructing the flux-rope topology using the FOTE method. *Science China Technological Sciences*, *62*, 144–150. <https://doi.org/10.1007/s11431-017-9201-1>
- Cranmer, S. R., van Ballegoijen, A. A., & Edgar, R. J. (2007). Self-consistent coronal heating and solar wind acceleration from anisotropic magnetohydrodynamic turbulence. *The Astrophysical Journal Supplement Series*, *171*, 520–551. <https://doi.org/10.1086/518001>
- Dahlin, J. T., Drake, J. F., & Swisdak, M. (2014). The mechanisms of electron heating and acceleration during magnetic reconnection. *Physics of Plasmas*, *21*, 092304. <https://doi.org/10.1063/1.4894484>
- Dong, C. F., Wang, L., Huang, Y. M., Comisso, L., & Bhattacharjee, A. (2018). Role of the plasmoid instability in magnetohydrodynamic turbulence. *Physical Review Letters*, *121*, 165101. <https://doi.org/10.1103/physrevlett.121.165101>
- Drake, J. F., Swisdak, M., Che, H., & Shay, M. A. (2006). Electron acceleration from contracting magnetic islands during reconnection. *Nature*, *443*, 553–556. <https://doi.org/10.1038/nature05116>
- Egedal, J., Daughton, W., & Le, A. (2012). Large-scale electron acceleration by parallel electric fields during magnetic reconnection. *Nature Physics*, *8*, 321–324. <https://doi.org/10.1038/nphys2249>

- Ergun, R. E., Tucker, S., Westfall, J., Goodrich, K. A., Malaspina, D. M., Summers, D., et al. (2016). The axial double probe and fields signal processing for the MMS mission. *Space Science Reviews*, 199, 167–188. <https://doi.org/10.1007/s11214-014-0115-x>
- Eriksson, E., Vaivads, A., Alm, L., Graham, D. B., Khotyaintsev, Y. V., & Andre, M. (2020). Electron acceleration in a magnetotail reconnection outflow region using magnetospheric multiscale data. *Geophysical Research Letters*, 47, e2019GL085080. <https://doi.org/10.1029/2019gl085080>
- Fargette, N., Lavraud, B., Øieroset, M., Phan, T. D., Toledo-Redondo, S., Kieokaew, R., et al. (2020). On the ubiquity of magnetic reconnection inside flux transfer event-like structures at the Earth's magnetopause. *Geophysical Research Letters*, 47, e2019GL086726. <https://doi.org/10.1029/2019gl086726>
- Fu, H. S., Cao, J. B., Vaivads, A., Khotyaintsev, Y. V., Andre, M., Dunlop, M., et al. (2016). Identifying magnetic reconnection events using the FOTE method. *Journal of Geophysical Research: Space Physics*, 121, 1263–1272. <https://doi.org/10.1002/2015ja021701>
- Fu, H. S., Khotyaintsev, Y. V., André, M., & Vaivads, A. (2011). Fermi and betatron acceleration of suprathermal electrons behind dipolarization fronts. *Geophysical Research Letters*, 38, L16104. <https://doi.org/10.1029/2011gl048528>
- Fu, H. S., Vaivads, A., Khotyaintsev, Y. V., André, M., Cao, J. B., Olshevsky, V., et al. (2017). Intermittent energy dissipation by turbulent reconnection. *Geophysical Research Letters*, 44, 37–43. <https://doi.org/10.1002/2016gl071787>
- Fu, X. R., Lu, Q. M., & Wang, S. (2006). The process of electron acceleration during collisionless magnetic reconnection. *Physics of Plasmas*, 13, 012309. <https://doi.org/10.1063/1.2164808>
- Huang, C., Wu, M., Lu, Q., Wang, R., & Wang, S. (2015). Electron acceleration in the dipolarization front driven by magnetic reconnection. *Journal of Geophysical Research: Space Physics*, 120, 1759–1765. <https://doi.org/10.1002/2014ja020918>
- Huang, S. Y., Sahraoui, F., Retino, A., Le Contel, O., Yuan, Z. G., Chasapis, A., et al. (2016). MMS observations of ion-scale magnetic island in the magnetosheath turbulent plasma. *Geophysical Research Letters*, 43, 7850–7858. <https://doi.org/10.1002/2016gl070033>
- Kacem, I., Jacquy, C., Génot, V., Lavraud, B., Vernisse, Y., Marchaudon, A., et al. (2018). Magnetic reconnection at a thin current sheet separating two interlaced flux tubes at the Earth's magnetopause. *Journal of Geophysical Research: Space Physics*, 123, 1779–1793. <https://doi.org/10.1002/2017ja024537>
- Karimabadi, H., Roytershteyn, V., Vu, H. X., Omelchenko, Y. A., Scudder, J., Daughton, W., et al. (2014). The link between shocks, turbulence, and magnetic reconnection in collisionless plasmas. *Physics of Plasmas*, 21, 062308. <https://doi.org/10.1063/1.4882875>
- Karimabadi, H., Roytershteyn, V., Wan, M., Matthaeus, W. H., Daughton, W., Wu, P., et al. (2013). Coherent structures, intermittent turbulence, and dissipation in high-temperature plasmas. *Physics of Plasmas*, 20, 012303. <https://doi.org/10.1063/1.4773205>
- Lavraud, B., Zhang, Y. C., Vernisse, Y., Gershman, D. J., Dorelli, J., Cassak, P. A., et al. (2016). Currents and associated electron scattering and bouncing near the diffusion region at Earth's magnetopause. *Geophysical Research Letters*, 43, 3042–3050. <https://doi.org/10.1002/2016gl068359>
- Lindqvist, P.-A., Olsson, G., Torbert, R. B., King, B., Granoff, M., Rau, D., et al. (2016). The spin-plane double probe electric field instrument for MMS. *Space Science Reviews*, 199, 137–165. [https://doi.org/10.1007/978-94-024-0861-4\\_6](https://doi.org/10.1007/978-94-024-0861-4_6)
- Lu, Q. M., Wang, H. Y., Huang, K., Wang, R. S., & Wang, S. (2018). Formation of power law spectra of energetic electrons during multiple X line magnetic reconnection with a guide field. *Physics of Plasmas*, 25, 072126. <https://doi.org/10.1063/1.5034012>
- Lu, Q. M., Wang, H. Y., Wang, X. Y., Lu, S., Wang, R. S., Gao, X. L., & Wang, S. (2020). Turbulence-driven magnetic reconnection in the magnetosheath downstream of a quasi-parallel shock: A three-dimensional global hybrid simulation. *Geophysical Research Letters*, 47, e2019GL085661. <https://doi.org/10.1029/2019gl085661>
- Lu, S., Angelopoulos, V., Artemyev, A. V., Pritchett, P. L., Liu, J., Runov, A., et al. (2019). Turbulence and particle acceleration in collisionless magnetic reconnection: Effects of temperature inhomogeneity across pre-reconnection current sheet. *The Astrophysical Journal*, 878, 109. <https://doi.org/10.3847/1538-4357/ab1f6b>
- Lu, S., Artemyev, A. V., Angelopoulos, V., & Pritchett, P. L. (2020). Energetic electron acceleration by ion-scale magnetic islands in turbulent magnetic reconnection: Particle-in-cell simulations and ARTEMIS observations. *The Astrophysical Journal*, 896z, 105. <https://doi.org/10.3847/1538-4357/ab908e>
- Øieroset, M., Phan, T. D., Drake, J. F., Eastwood, J. P., Fuselier, S. A., Strangeway, R. J., et al. (2019). Reconnection with magnetic flux pileup at the interface of converging jets at the magnetopause. *Geophysical Research Letters*, 46, 1937–1946. <https://doi.org/10.1029/2018gl080994>
- Oka, M., Phan, T.-D., Krucker, S., Fujimoto, M., & Shinohara, I. (2010). Electron acceleration by multi-island coalescence. *The Astrophysical Journal*, 714, 915–926. <https://doi.org/10.1088/0004-637x/714/1/915>
- Phan, T. D., Eastwood, J. P., Shay, M. A., Drake, J. F., Sonnerup, B. U. Ö., Fujimoto, M., et al. (2018). Electron magnetic reconnection without ion coupling in Earth's turbulent magnetosheath. *Nature*, 557, 202–206. <https://doi.org/10.1038/s41586-018-0091-5>
- Pollock, C., Moore, T., Jacques, A., Burch, J., Gliese, U., Saito, Y., et al. (2016). Fast plasma investigation for magnetospheric multiscale. *Space Science Reviews*, 199, 331–406. <https://doi.org/10.1007/s11214-016-0245-4>
- Pu, Z. Y., Raeder, J., Zhong, J., Bogdanova, Y. V., Dunlop, M., Xiao, C. J., et al. (2013). Magnetic topologies of an in vivo FTE observed by Double Star/TC-1 at Earth's magnetopause. *Geophysical Research Letters*, 40, 3502–3506. <https://doi.org/10.1002/grl.50714>
- Retino, A., Sundkvist, D., Vaivads, A., Mozer, F., André, M., & Owen, C. J. (2007). In situ evidence of magnetic reconnection in turbulent plasma. *Nature Physics*, 3, 235–238. <https://doi.org/10.1038/nphys574>
- Roux, A., Robert, P., Fontaine, D., Contel, O. L., Canu, P., & Louarn, P. (2015). What is the nature of magnetosheath FTEs? *Journal of Geophysical Research: Space Physics*, 120, 4576–4595. <https://doi.org/10.1002/2015ja020983>
- Russell, C. T., Anderson, B. J., Baumjohann, W., Bromund, K. R., Dearborn, D., Fischer, D., et al. (2016). The Magnetospheric Multiscale magnetometers. *Space Science Reviews*, 199, 189–256. <https://doi.org/10.1007/s11214-014-0057-3>
- Russell, C. T., & Elphic, R. C. (1978). Initial ISEE magnetometer results: Magnetopause observations. *Space Science Reviews*, 22, 681–715. <https://doi.org/10.1007/bf00212619>
- Sahraoui, F., Belmont, G., Rezeau, L., Cornilleau-Wehrin, N., Pincon, J. L., & Balogh, A. (2006). Anisotropic turbulent spectra in the terrestrial magnetosheath as seen by the Cluster spacecraft. *Physical Review Letters*, 96, 075002. <https://doi.org/10.1103/physrevlett.96.075002>
- Schekochihin, A. A., Cowley, S. C., Dorland, W., Hammett, G. W., Howes, G. G., Quataert, E., & Tatsuno, T. (2009). Astrophysical gyrokinetics: Kinetic and fluid turbulent cascades in magnetized weakly collisional plasmas. *The Astrophysical Journal Supplement Series*, 182, 310–377. <https://doi.org/10.1088/0067-0049/182/1/310>
- Schwartz, S. J. (1998). Shock and discontinuity normals, mach numbers and related parameters. In G. Paschmann, & P. W. Daly (Eds.), *Analysis methods for multi-spacecraft data* (pp. 249–270). Bern, Switzerland: International Space Science Institute.
- Servidio, S., Matthaeus, W. H., Shay, M. A., Cassak, P. A., & Dmitruk, P. (2009). Magnetic reconnection in two-dimensional magnetohydrodynamic turbulence. *Physical Review Letters*, 102, 115003. <https://doi.org/10.1103/physrevlett.102.115003>
- Shen, C., Li, X., Dunlop, M., Shi, Q. Q., Liu, Z. X., Lucek, E., & Chen, Z. Q. (2007). Magnetic field rotation analysis and the applications. *Journal of Geophysical Research*, 112, A06211. <https://doi.org/10.1029/2005JA011584>

- Stawarz, J. E., Eastwood, J. P., Phan, T. D., Gingell, I. L., Shay, M. A., Burch, J. L., et al. (2019). Properties of the turbulence associated with electron-only magnetic reconnection in Earth's magnetosheath. *The Astrophysical Journal Letters*, *877*, L37. <https://doi.org/10.3847/2041-8213/ab21c8>
- Sundkvist, D., Retino, A., Vaivads, A., & Bale, S. D. (2007). Dissipation in turbulent plasma due to reconnection in thin current sheets. *Physical Review Letters*, *99*, 025004. <https://doi.org/10.1103/physrevlett.99.025004>
- Sun, W. J., Slavin, J. A., Tian, A. M., Bai, S. C., Poh, G. K., Akhavan-Tafti, M., et al. (2019). MMS study of the structure of ion-scale flux ropes in the Earth's cross-tail current sheet. *Geophysical Research Letters*, *46*, 6168–6177. <https://doi.org/10.1029/2019gl083301>
- Voros, Z., Yordanova, E., Varsani, A., Genestreti, K. J., Khotyaintsev, Yu. V., Li, W., et al. (2017). MMS observation of magnetic reconnection in the turbulent magnetosheath. *Journal of Geophysical Research: Space Physics*, *122*, 11442–11467. <https://doi.org/10.1002/2017ja024535>
- Wang, H., Lu, Q., Huang, C., & Wang, S. (2016). The mechanisms of electron acceleration during multiple X line magnetic reconnection with a guide field. *The Astrophysical Journal*, *821*, 84. <https://doi.org/10.3847/0004-637x/821/2/84>
- Wang, R., Lu, Q., Khotyaintsev, Y. V., Volwerk, M., Du, A., Nakamura, R., et al. (2014). Observation of double layer in the separatrix region during magnetic reconnection. *Geophysical Research Letters*, *41*, 4851–4858. <https://doi.org/10.1002/2014gl061157>
- Wang, R., Lu, Q., Nakamura, R., Baumjohann, W., Russell, C. T., Burch, J. L., et al. (2017). Interaction of magnetic flux ropes via magnetic reconnection observed at the magnetopause. *Journal of Geophysical Research: Space Physics*, *122*, 10436–10447. <https://doi.org/10.1002/2017ja024482>
- Wang, R., Lu, Q., Nakamura, R., Huang, C., Du, A., Guo, F., et al. (2016). Coalescence of magnetic flux ropes in the ion diffusion region of magnetic reconnection. *Nature Physics*, *12*, 263–267. <https://doi.org/10.1038/nphys3578>
- Wang, S., Wang, R., Lu, Q. M., Fu, H. S., & Wang, S. (2020). Direct evidence of secondary reconnection inside filamentary currents of magnetic flux ropes during magnetic reconnection. *Nature Communications*, *11*, 3964. <https://doi.org/10.1038/s41467-020-17803-3>
- Wang, S., Wang, R., Yao, S. T., Lu, Q., Russell, C. T., & Wang, S. (2019). Anisotropic electron distributions and whistler waves in a series of the flux transfer events at the magnetopause. *Journal of Geophysical Research: Space Physics*, *124*, 1753–1769. <https://doi.org/10.1029/2018ja026417>
- Wan, M., Matthaeus, W. H., Karimabadi, H., Roytershteyn, V., Shay, M., Wu, P., et al. (2012). Intermittent dissipation at kinetic scales in collisionless plasma turbulence. *Physical Review Letters*, *109*, 195001. <https://doi.org/10.1103/physrevlett.109.195001>
- Wilder, F. D., Ergun, R. E., Burch, J. L., Ahmadi, N., Eriksson, S., Phan, T. D., et al. (2018). The role of the parallel electric field in electron-scale dissipation at reconnecting currents in the magnetosheath. *Journal of Geophysical Research: Space Physics*, *123*, 6533–6547. <https://doi.org/10.1029/2018ja025529>
- Wu, M., Lu, Q., Volwerk, M., Vörös, Z., Zhang, T., Shan, L., & Huang, C. (2013). A statistical study of electron acceleration behind the dipolarization fronts in the magnetotail. *Journal of Geophysical Research: Space Physics*, *118*, 4804–4810. <https://doi.org/10.1002/jgra.50456>
- Yang, Y. Y., Shen, C., Zhang, Y. C., Rong, Z. J., Li, X., Dunlop, M., et al. (2014). The force-free configuration of flux ropes in geomagnetotail: Cluster observations. *Journal of Geophysical Research: Space Physics*, *119*. <https://doi.org/10.1002/2013ja019642>
- Yao, S. T., Hamrin, M., Shi, Q. Q., Yao, Z. H., Degeling, A. W., Zong, Q.-G., et al. (2020). Propagating and dynamic properties of magnetic dips in the dayside magnetosheath: MMS observations. *Journal of Geophysical Research: Space Physics*, *125*, e2019JA026736. <https://doi.org/10.1029/2019ja026736>
- Yao, S. T., Shi, Q. Q., Guo, R. L., Yao, Z. H., Fu, H. S., Degeling, A. W., et al. (2020). Kinetic-scale flux rope in the magnetosheath boundary layer. *The Astrophysical Journal*, *897*, 137. <https://doi.org/10.3847/1538-4357/ab9620>
- Yao, S. T., Shi, Q. Q., Guo, R. L., Yao, Z. H., Tian, A. M., Degeling, A. W., et al. (2018). Magnetospheric multiscale observations of electron scale magnetic peak. *Geophysical Research Letters*, *45*, 527–537. <https://doi.org/10.1002/2017gl075711>
- Yordanova, E., Vörös, Z., Varsani, A., Graham, D. B., Norgren, C., Khotyaintsev, Y. V., et al. (2016). Electron scale structures and magnetic reconnection signatures in the turbulent magnetosheath. *Geophysical Research Letters*, *43*, 5969–5978. <https://doi.org/10.1002/2016gl069191>
- Zenitani, S., Hesse, M., Klimas, A., & Kuznetsova, M. (2011). New measure of the dissipation region in collisionless magnetic reconnection. *Physical Review Letters*, *106*, 195003. <https://doi.org/10.1103/physrevlett.106.195003>
- Zhao, Y., Wang, R., Lu, Q. M., Du, A. M., Yao, Z. H., & Wu, M. Y. (2016). Coalescence of magnetic flux ropes observed in the tailward high-speed flows. *Journal of Geophysical Research: Space Physics*, *121*, 10898–10909. <https://doi.org/10.1002/2016ja023526>
- Zhong, J., Pu, Z. Y., Dunlop, M. W., Bogdanova, Y. V., Wang, X. G., Xiao, C. J., et al. (2013). Three-dimensional magnetic flux rope structure formed by multiple sequential X-line reconnection at the magnetopause. *Journal of Geophysical Research: Space Physics*, *118*, 1904–1911. <https://doi.org/10.1002/jgra.50281>
- Zhong, Z. H., Zhou, M., Tang, R. X., Deng, X. H., Turner, D. L., Cohen, I. J., et al. (2020). Direct evidence for electron acceleration within ion-scale flux rope. *Geophysical Research Letters*, *47*, e2019GL085141. <https://doi.org/10.1029/2019gl085141>
- Zhou, M., Berchem, J., Walker, R. J., El-Alaoui, M., Deng, X., Cazzola, E., et al. (2017). Coalescence of macroscopic flux ropes at the subsolar magnetopause: Magnetospheric Multiscale observations. *Physical Review Letters*, *119*, 055101. <https://doi.org/10.1103/physrevlett.119.055101>
- Zhou, M., Pang, Y., Deng, X., Huang, S., & Lai, X. (2014). Plasma physics of magnetic island coalescence during magnetic reconnection. *Journal of Geophysical Research: Space Physics*, *119*, 6177–6189. <https://doi.org/10.1002/2013ja019483>
- Zong, Q. G., Fritz, T. A., Pu, Z. Y., Fu, S. Y., Baker, D. N., Zhang, H., et al. (2004). Cluster observations of earthward flowing plasmoid in the tail. *Geophysical Research Letters*, *31*, L18803. <https://doi.org/10.1029/2004gl020692>